Steel and Composite Structures, *Vol. 30, No. 6 (2019) 591-601*
DOI: https://doi.org/10.12989/scs.2019.30.6.591

Experimental and analytical investigations of CFFT columns with and without FRP bars under concentric compression

Qasim S. Khan [1a], M. Neaz Sheikh [2b] and Muhammad N.S. Hadi [*2]

[1] *Civil Engineering Department, University of Engineering and Technology, Lahore, Pakistan*
[2] *School of Civil, Mining and Environmental Engineering, University of Wollongong, Australia*

(*Received August 22, 2018, Revised February 6, 2019, Accepted March 13, 2019*)

Abstract. This research study investigates experimentally and analytically the axial compressive behaviour of Concrete Filled Fiber Reinforced Polymer Tube (CFFT) columns with and without Fiber Reinforced Polymer (FRP) bars. The experimental program comprises five circular columns of 204-206 mm outer diameter and 800-812 mm height. All columns were tested under concentric axial compressive loads. It was found that CFFT columns with and without FRP bars achieved higher peak axial compressive loads and corresponding axial deformations than conventional steel reinforced concrete (RC) column. The contribution of FRP bars was about 12.1% of the axial compressive loads carried by CFFT columns reinforced with FRP bars. Axial load-axial deformation ($P - \delta$) curves of CFFT columns were analytically constructed, which mapped well with the experimental $P - \delta$ curves. Also, an equation was proposed to predict the axial compressive load capacity of CFFT columns with and without FRP bars, which adequately considers the contributions of the circumferential confinement provided by FRP tubes and lower ultimate strength of FRP bars in compression than in tension.

Keywords: CFFT; FRP bars; axial load-deformation curve; axial load carrying capacity; columns

1. Introduction

Steel bar Reinforced Concrete (RC) columns are widely used in buildings and bridges to transfer loads from superstructures to substructures. A major drawback of steel RC columns is the rusting of steel reinforcement over the design life cycle of the structure, which severely affects the serviceability of the RC columns particularly in harsh and corrosive, coastal environments. Fiber Reinforced Polymer (FRP) reinforcement has recently surfaced as one of the potential alternatives of steel reinforcement due to lower self-weight, and higher ultimate strength in tension and superior rust resistance of FRP reinforcement compared to steel reinforcement (Pantelides *et al*. 2013, Aslani *et al*. 2015, Park and Yoo 2015, Thomas and Ramadass 2015, Wang *et al*. 2017, Khan *et al*. 2018a, Ramezanpour *et al*. 2018, Shahraki *et al*. 2018, Wang *et al*. 2018).

A review of available research studies exhibited that both modulus of elasticity (MOE) and ultimate strength of fibers of FRP bars are lower in compression than in tension. Chaallal and Benmokrane (1993) reported that the compressive MOE of FRP bars was 77-97% of their tensile MOE. Also, the ultimate compressive strength of FRP bars was 78-80% of their ultimate tensile strength. Kobayashi and Fujisaki (1995) noted that the ultimate compressive strengths of Glass FRP (GFRP), Carbon FRP (CFRP) and Aramid FRP (AFRP) bars were 30-40%, 30-50% and 10% of the respective ultimate tensile strengths. Deitz *et al*. (2003) tested GFRP bars of 15 mm diameter in compression and reported that the ultimate compressive strength of GFRP bar was about 50% of its ultimate tensile strength.

Until today, only a limited number of experimental investigations reported the axial compressive behavior of FRP bar RC columns. The FRP bar RC columns were found to carry lower axial compressive loads than the steel RC columns. The contribution of FRP bars in the axial compressive load capacity of FRP bar RC columns was found to be lower than the contribution of steel bars in axial compressive load capacity of steel RC columns. Alsayed *et al*. (1999) noted that rectangular GFRP bar RC columns carried 13% smaller axial compressive loads than rectangular steel RC columns. De Luca *et al*. (2010) and Tobbi *et al*. (2012) noted that GFRP bars carried 2.9-10% of the axial compressive loads carried by GFRP bar reinforced square concrete columns. Afifi *et al*. (2014a) reported that GFRP bars carried 5-10% of the axial compressive loads carried by circular GFRP bar RC columns. Afifi *et al*. (2014b) reported that CFRP bars carried 13% of axial compressive loads carried by circular CFRP bar RC columns. Hadi *et al*. (2016) found that GFRP bars carried 12% of the axial compressive loads carried by circular GFRP bar RC columns. Hadhood *et al*. (2016) reported that circular CFRP bar RC columns exhibited 4% smaller axial compressive load capacity than steel RC columns at different axial load eccentricities. Due to lack of adequate research studies, CSA S806-12 (2012) does not consider the contribution of FRP bars in axial compressive load capacity

*Corresponding author, Associate Professor,
E-mail: mhadi@uow.edu.au
[a] Ph.D., Assistant Professor, E-mail: qasimkhan@uet.edu.pk
[b] Associate Professor

ISSN: 1229-9367 (Print), 1598-6233 (Online)

of FRP bar RC columns. Also, ACI 440.1R-06 (2006) does not allow providing longitudinal FRP bars in RC columns. However, in the recent edition of ACI 440.1R-15 (2015) the suggestions about not using longitudinal FRP bars in RC columns were excluded.

The Concrete Filled Fiber reinforced polymer Tube (CFFT) column was studied as a potential substitute of the steel RC column in the last two decades. The CFFT serves as formwork for new column construction along with increased rust resistance even in harsh, corrosive environments. The experimental work into the axial compressive behavior of unreinforced CFFT columns showed that FRP tube significantly increased the strength and ductility of the confined concrete (Mirmiran *et al*. 1998, Hong and Kim 2004, Ozbakkaloglu and Oehlers 2008, Park *et al*. 2011, Ozbakkaloglu and Vincent 2013, Vincent and Ozbakkaloglu 2013a, b, Hadi *et al*. 2016). Khan *et al*. (2016) presented a comprehensive review of the axial compressive behavior of unreinforced CFFT columns and also proposed design-oriented models to determine the confined concrete strength and ultimate confined concrete strain of unreinforced CFFT columns under axial compression.

A limited number of experimental investigations explored the potential benefits of steel reinforced CFFT columns under axial compression. Mohamed and Masmoudi (2008) reported that steel reinforcement enhanced the axial compressive load capacity and ductility of steel reinforced CFFT columns. Mohamed and Masmoudi (2010) proposed an equation to calculate the axial compressive load capacity of steel reinforced CFFT columns. To the knowledge of the authors, the experimental investigations of FRP bar reinforced CFFT columns under concentric axial compression are still very limited. Khan *et al*. (2017) reported that GFRP bar reinforced GFRP-CFFT columns resisted higher peak axial compressive loads and corresponding higher axial and lateral deformations than unreinforced GFRP-CFFT columns and steel RC columns under axial compression. Khan *et al*. (2018b) noted that CFRP bar reinforced CFRP-CFFT columns under axial compression can be used as a substitute of steel RC columns and CFRP bars can serve as a longitudinal reinforcement for CFRP-CFFT columns similar to steel bars in steel RC columns. It is apparent from the review of literature that more experimental and analytical studies are required to adequately understand the behavior of FRP bar reinforced CFFT columns under axial compression. Moreover, none of the studies reviewed above experimentally and analytically explored the axial compressive behavior of CFRP-CFFT columns reinforced with CFRP bars and GFRP-CFFT columns reinforced with GFRP bars. This study reports the experimental and analytical axial load-axial deformation behavior of CFFT columns with and without FRP bars under concentric axial compression as a viable alternative of steel RC columns. Moreover, an equation is proposed to calculate the axial load carrying capacity of FRP bar reinforced CFFT columns based on the test results presented in this study.

2. Experimental program

The experimental program reported in this study is part of the current research investigations about the application of advanced composites in sustainable infrastructure construction at the School of Civil, Mining and Environmental Engineering (CME), University of Wollongong (UOW), Australia. In the experimental program, a reference steel Reinforced Concrete (RC) column, an unreinforced CFRP-CFFT column, an unreinforced GFRP-CFFT column, a CFRP bar reinforced CFRP-CFFT column, and a GFRP bar reinforced GFRP-CFFT column were constructed and tested under concentric axial compression at the Structural Engineering Laboratories, School of CME, UOW, Australia. The test columns of 200-203 mm inner diameter and 800-812 mm height were selected considering the available testing facilities. The height to diameter ratio of all the columns was fixed as 4. The reference steel RC column was reinforced, with six deformed steel bars of 12 mm diameter and with 10 mm diameter steel helix with outer diameter of 165 mm and center to center spacing of 60 mm. The reference column was identified as Column REF. The CFFT columns were identified according to the types of FRP tube and FRP bar. The CFRP tube was identified as CT and GFRP tube was identified as GT. The CFRP bar was identified as CR and GFRP bar was identified as GR. Column CT was unreinforced CFRP tube confined concrete. Column GT was unreinforced GFRP tube confined concrete. Column CTCR was CFRP tube confined concrete reinforced with six CFRP bars of 15 mm diameter. Column GTGR was GFRP tube confined concrete reinforced with six GFRP bars of 15.9 mm diameter.

2.1 Material properties

2.1.1 Properties of steel and FRP reinforcement

The tensile properties of steel bars were determined in accordance with the guidelines in AS 1391-2007 (2007). The measured tensile strengths of 10 mm diameter and 12 mm diameter steel bars were 400 MPa and 600 MPa, respectively. Smooth CFRP bars and sand coated GFRP bars with all the fiber orientations along the longitudinal direction (pultruded) were used as reinforcing bars in CFFT columns. The CFRP bar comprised 60% fibers and 40% resin by volume (CST Composites 2014). The GFRP bar comprised 73% fibers and 27% resin by volume (V-Rod). The diameters of FRP bars were measured in accordance with the guidelines for the immersion test outlined in ISO 104061-1-15 (2015). For CFRP bar, nominal and measured diameters (15 mm) were similar. For GFRP bar, the nominal diameter (15.9 mm) and the measured diameter (19.3 mm) were different due to the sand coat, which was applied to enhance the bonding of GFRP bars with the surrounding concrete. It was noted that sand coat did not contribute to the strength of bar. Hence, the nominal diameter of GFRP bar was considered in calculating ultimate strengths.

Table 1 Mechanical properties of tested FRP bars in compression

*FRP bar ID	Nominal diameter, D (mm)	+Measured diameter, D (mm)	Ultimate strength, $f_{fu,c}$ (MPa)	Tangent modulus of elasticity, E (GPa)	Ultimate strain, $\varepsilon_{fu,c}$ (%)
CR-C-1			609	49.2	1.45
CR-C-2			599	50.0	1.95
CR-C-3	15.0	15.0	618	50.0	1.56
CR-C-4			586	46.4	1.62
CR-C-5			571	49.7	1.60
GR-C-1			903	43.3	2.88
GR-C-2			804	43.3	2.78
GR-C-3	15.9	19.3	743	41.4	2.58
GR-C-4			784	42.0	2.55
GR-C-5			995	40.0	3.04

* CR = CFRP bar, GR = GFRP bar and C = Compression test
+Dia. measured according to ISO (2015)

Table 2 Mechanical properties of tested FRP bars in tension

*FRP bar ID	Nominal diameter, D (mm)	+Measured diameter, D (mm)	Ultimate strength, f_{fu} (MPa)	Tangent modulus of elasticity, E (GPa)	Ultimate strain, ε_{fu} (%)
CR-T-1			1147	94.6	2.15
CR-T-2	15.0	15.0	1128	86.9	2.29
CR-T-3			1195	86.7	2.43
GR-T-1			1410	54.8	5.11
GR-T-2	15.9	19.3	1468	57.5	5.04
GR-T-3			1308	55.6	4.66

* CR = CFRP bar, GR = GFRP bar and C = Compression test
+Dia. measured according to ISO (2015)

The FRP bars were identified based on type of FRP bar (CR or GR), type of testing arrangement (compression or tension) and FRP bar number tested in specific series. For example, CR-C-2 denotes a CFRP bar tested in compression and was the second CFRP bar in the series. Five specimens from each of CFRP bar (gauge length 60 mm) and GFRP bar (gauge length 80 mm) were tested in compression. The compression testing of both CFRP and GFRP bars was conducted using the procedure outlined in ASTM D695-10 (2010) in the 100 kN Instron testing machine. The observed failure in the tested CFRP and GFRP bars was attributed to separation of fibers, which might be because of the resin failure rather than buckling of fibers. The experimental results of CFRP and GFRP bars tested in compression are presented in Table 1. The mean compressive strengths of, CFRP bar was 596 MPa and GFRP bar was 846 MPa. Three specimens from each of CFRP bar (gauge length 600 mm) and GFRP bar (gauge length 635 mm) were tested in tension. The tension testing of both CFRP and GFRP bars was conducted using the procedure outlined in ASTM D7205/D7205-16 (2016) in the 500 kN Instron testing machine. The observed failure in the tested CFRP and GFRP bars was because of the tensile splitting of fibers in the gauge length. The experimental results of CFRP and GFRP bars tested in tension are presented in Table 2. The mean tensile strengths of, CFRP bar was 1157 MPa and GFRP bar was 1395 MPa. The lower ultimate tensile strength of CFRP bar than that of GFRP bar could be because CFRP bars comprised significantly lower percentage of fibers than that of GFRP bars. The nominal diameter of CFRP bar (15 mm) was smaller than the nominal diameter of GFRP bar (15.9 mm).

2.1.2 Properties of FRP tube

The properties (FRP tube thickness, modulus of elasticity and ultimate tensile strength) of CFRP and GFRP tubes were selected to attain similar confining capacities of CFFT columns. The CFRP tubes of 0.5 mm nominal thickness and GFRP tubes of 1.50 mm nominal thickness, respectively, were chosen for CFRP-CFFT and GFRP-CFFT columns. The orientations of fibers in both types of the tube were selected with the inner fiber layers oriented 90° to the longitudinal axis (circumferential direction) and outer fiber layers oriented ±60° to the longitudinal axis (skew direction) (CST Composites 2014). The mechanical properties of CFRP and GFRP tubes were determined based on the mechanical properties of fibers and resins provided by the manufacturers using mixtures rule for FRP composites and details are presented in Table 3.

2.1.3 Column preparation

For Column REF, a PVC pipe of 200 mm internal

Table 3 Computed mechanical properties of FRP tubes

FRP tube type	Circumferential direction		Longitudinal direction	
	Modulus of elasticity E_c (GPa)	Ultimate tensile strength $f_{fu,c}$ (MPa)	Modulus of elasticity E_l (GPa)	Ultimate tensile strength $f_{fu,l}$ (MPa)
Carbon	54.0	1188.0	16.2	142.6
Glass	18.0	810.0	5.4	92.2

diameter and 800 mm height was vertically positioned in a timber formwork. In Column REF, steel bars were tied to the inner side of steel helix, and a 20 mm concrete cover at the side and a 15 mm cover to the concrete at both ends were provided. For CFFT (CT, GT, CTCR and GTGR) columns, FRP tubes served as formworks, shear and longitudinal reinforcement and FRP tubes were vertically positioned in a timber formwork. In FRP bar reinforced CFFT columns, six FRP bars were attached on the inner side 60° apart along the circumferential direction. In columns CTCR and GTGR, the reinforcement arrangement was similar to steel RC columns, and a 15 mm cover to the concrete at both ends was provided.

The test columns were constructed with a batch of ready mix concrete. The 28-day average compressive concrete strength tested according to AS 1012.9-1999 (1999) was 37 MPa. All columns were cured for 28 days. After curing, the column ends up to 100 mm height were strengthened with two layers of 0.5 mm thick CFRP sheet wrapped in the circumferential direction to prevent premature compression failures at the ends during testing.

2.2 Instrumentation and test methodology

The test columns were externally and internally instrumented to determine deformations and strains in the reinforcement. Two Linear Variable Displacement Transducers (LVDTs) were fixed 180° apart on the two opposite corners of the testing machine to determine deformations in the test columns in the axial direction (Fig. 1). In Column REF, a pair of strain gauge was fixed 180° apart on two steel bars at the middle height to determine axial strain in steel bars and a pair of strain gauge was fixed180° apart on steel helix at the middle height to determine lateral strains in steel helix. A pair of strain gauge was fixed 180° apart on FRP tubes at the middle height in the axial direction to determine axial strains in FRP tubes and a pair of strain gauge was fixed 180° apart on FRP tubes at the middle height in the circumferential direction to determine circumferential strains in FRP tubes. Columns CTCR and GTGR were instrumented with two pairs of strain gauges fixed on two FRP bars 180° apart in the axial direction at the middle height to determine strains in FRP bars.

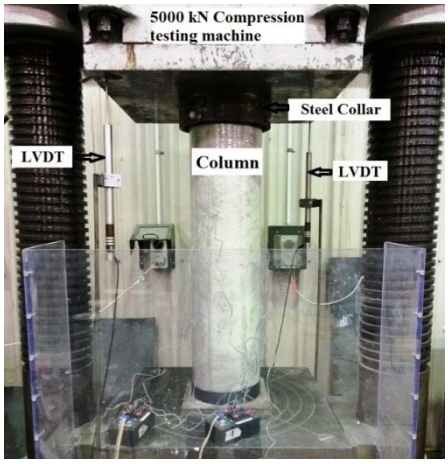

Fig. 1 Setup for testing of columns in 5000 kN Denison Compression Testing Machine

All columns were tested in the 5000 kN Denison Compression testing machine under concentric axial compression (Fig. 1). All test columns were initially loaded to 100 kN and then unloaded to 20 kN under the force-controlled load applications at a rate of 50 kN/min.

Fig. 2 Observed failures in tested columns

Afterwards, testing was continued at a rate of 0.3 mm/min until the failure of column under the displacement-controlled load applications.

2.3 Observed failure modes

The tested CFFT columns failed in a brittle manner with rupturing of FRP tube and crushing of concrete. Column REF failed due to spalling of concrete cover throughout the height of column and splitting of steel helix and buckling of longitudinal steel bars. Columns CT and GT failed due to rupturing of FRP tubes at the mid-height of the columns with loud snapping sounds of rupturing of fibers and crushing of concrete. Column CTCR failed due to rupturing of CFRP tube throughout the height of the column along with outward buckling of CFRP bars and crushing of concrete. Column GTGR failed due to rupturing of GFRP tube within the top one-third height of the column with outward buckling of GFRP bars and crushing of concrete (Fig. 2).

3. Test results and discussions

The test results of the columns in terms of peak axial compressive load (P) and corresponding axial deformation (δ), average axial and circumferential strains in FRP tube at middle height of the column at f_{co} and at peak axial load, and average axial strain in bars at middle height of the column at peak axial loads are reported in Table 4.

3.1 Axial load-strain behavior of CFFT

Axial load-axial strain behavior of CFFTs without FRP bars (CT and GT) and CFFTs reinforced with FRP bars (CTCR and GTGR) columns can be identified by two rising curves smoothly joined at transition point (Figs. 3(a) and (b)). The first rising curve showed a sharp rise in the applied axial compressive loads which produced increased micro-cracking in the confined concrete and hence increased lateral expansion of the confined concrete due to Poisson's effect. The increase in lateral expansion of the confined concrete resulted in increased circumferential confinement pressure applied by the confined concrete at the interface of FRP tube and concrete. As the lateral expansion of the confined concrete approached the critical axial compressive load (load corresponding to approximately the unconfined strength of concrete) of FRP tube confined concrete, the FRP tube confinement was activated i.e., initiation of the second curve (transition point). The FRP tube started confining the dilated concrete with increasing confinement pressure. The confinement pressure continued to increase with an increase in axial compressive load and dilated confined concrete continued to resist axial compressive load until the confining capacity of FRP tube was exhausted (rupture point). The gradient of the first curve depends on unconfined concrete strength while the gradient of the second curve depends on the confining capacity of FRP tube.

The axial strain at the transition point in CFRP tubes in Columns CT (0.26%) and CTCR (0.25%) were similar. However, the axial strain at the transition point in GFRP

Table 4 Details of experimental results in this study

Col. ID	(P), kN	(δ), mm	Average strains in circumferential reinforcement				Average strain in bars, %
			f_{co}, %		Peak axial load, %		
			Axial strain	Circumferential strain	Axial strain	Circumferential strain	
REF	1529	2.4	-	-	-	0.10	1.20
CT	1770	18.1	0.26	0.10	1.87	1.31	-
GT	1884	21.3	0.19	0.13	2.62	1.30	-
CTCR	2197	20.9	0.25	0.10	2.96	1.40	0.27
GTGR	2812	23.1	0.49	0.10	2.95	1.12	0.54

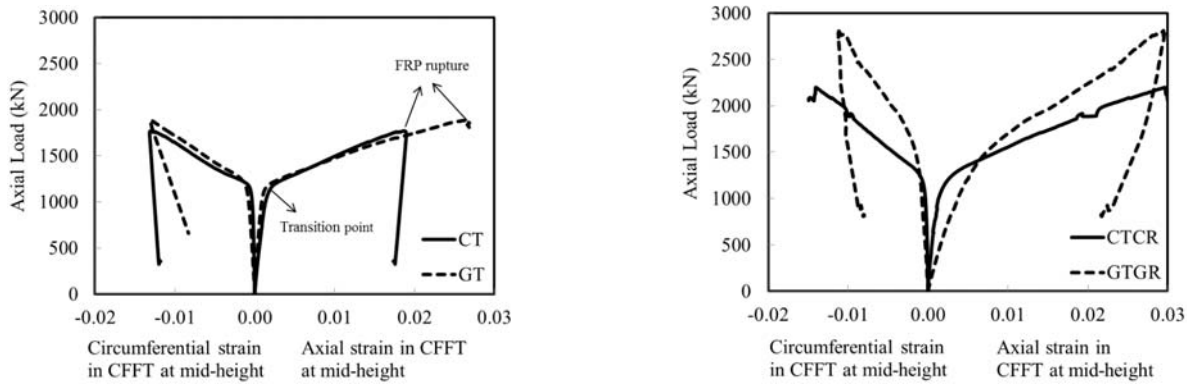

(a) Columns CT and GT

(b) Specimens CTCR and GTGR

Fig. 3 Axial load-axial strain and axial load-circumferential strain curve at the mid-height of (a) and (b)

tube in Column GTGR (0.49%) was 2.4 times the axial strain at the transition point in GFRP tube in Column GT (0.19%), which could be attributed to different locations of stress concentration within the tested columns (Figs. 3(a) and (b)). The circumferential strains at transition point in CFRP tubes in Columns CT (0.10%) and CTCR (0.10%) were similar. Moreover, the circumferential strains at the transition point in GFRP tubes in Columns GT (0.10%) and GTGR (0.13%) were also similar (Figs. 3(a) and (b)). The lower circumferential strains at the transition point in tested columns indicated that FRP confinement was less activated in confining the concrete.

The axial strain at rupture point in CFRP tube in Column CT (1.87%) was 36.8% smaller than the axial strain at rupture point in CFRP tube in Column CTCR (2.96%). The axial strain at rupture point in GFRP tube in Column GT (2.62%) was 11.2% smaller than the axial strain at rupture point in GFRP tube in Column GTGR (2.95%) (Figs. 3(a) and (b)). The circumferential strain in CFRP tube in Column CT (1.31%) was 6.4% smaller than the circumferential strain in CFRP tube in Column CTCR (1.40%). The circumferential strain in GFRP tube in Column GT (1.30%) was 13.8% smaller than the circumferential strain in GFRP tube in Column GTGR (1.12%) (Figs. 3(a) and (b)). The lower axial and circumferential strains at rupture point in FRP tubes in Columns CT and GT than Columns CTCR and GTGR could be attributed to the confinement effect of FRP bars in addition to the confinement provided by FRP tubes.

3.2 Influence of FRP tube

Columns CT and GT carried 15.8% and 23.2% larger axial compressive load capacity, respectively, than Column REF. The average circumferential strains in FRP tube at peak axial compressive load in Columns CT (1.31%) and GT (1.30%) were 13.2 and 13.1 times, respectively, of the average lateral strains in steel helix at peak axial compressive load in Column REF (0.10%) (Fig. 4). The larger circumferential strain at peak axial compressive load indicates the significantly higher confining capacity of FRP tubes than that of steel helix as two-thirds of the fibers in FRP tubes were oriented along the circumferential direction. It may also be because FRP tubes provide continuous circumferential confinement. In addition, FRPs have higher tensile strength than steel. However, Columns CT and GT ruptured in a brittle way with a sudden reduction in axial load as FRP composites are linear elastic until rupture.

3.3 Influence of FRP reinforcement

Axial load-axial strain response of bars in Columns REF, CTCR and GTGR is shown in Fig. 5. The measured axial strains in GFRP bars (0.54%) were two times of the measured axial strains in CFRP bars (0.27%) which indicated that both types of FRP bars effectively resisted the axial compressive loads in Columns CTCR and GTGR. However, CFRP and GFRP bars attained about 0.3-0.4 times of their ultimate tensile strength at the failure load. Columns CTCR and GTGR carried 43.8% and 83.9% greater axial compressive load capacity, respectively, than Column REF. The measured axial strains in steel bars at peak axial compressive loads were 4.4 and 2.2 times greater, respectively, than the measured axial strains in CFRP bars and GFRP bars. The higher effectiveness of steel bar than FRP bars was due to the higher modulus of elasticity (MOE) of steel than of FRPs. The axial compressive loads carried by FRP bars was calculated based on MOE of FRP bar, axial strain in FRP bar and cross-sectional area of FRP bar. The axial compressive loads carried by CFRP and GFRP bars were 11.7% and 12.5%, respectively, of the axial compressive load capacity of Columns CTCR and GTGR. The axial compressive loads carried by CFRP and GFRP bars are similar to the axial compressive loads carried by FRP bars reported in the literature (Afifi *et al*. 2014a, b). The axial compressive loads carried by steel bar was 26.2% of the axial compressive load capacity of Column REF. Columns CTCR and GTGR carried 24.2% and 49.3% greater axial compressive load capacity, respectively than Columns CT and GT. This was because of the longitudinal FRP bars in CFFT columns which were effective in resisting axial compressive loads.

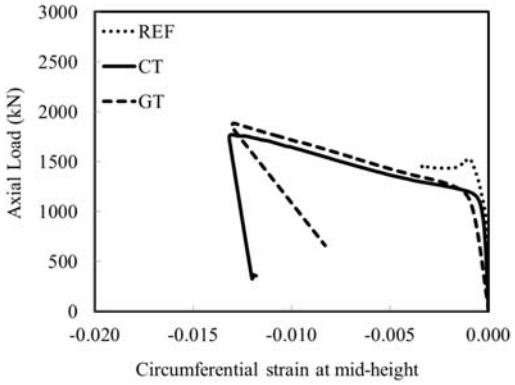

Fig. 4 Axial load-circumferential strain curves at the middle height of Columns REF, CT and GT

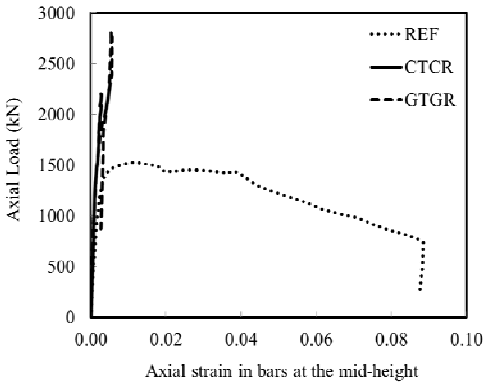

Fig. 5 Axial load-axial strain curves of bars at the middle height of Columns REF, CTCR and GTGR

4. Analytical axial load-axial deformation response of CFFT columns

The circumferential confinement pressure applied by FRP confinement on the concrete due to lateral expansion of the confined concrete under uniaxial compression is assumed to be uniformly distributed along the circumference of the confined concrete. An increasing lateral expansion of the confined concrete produces increasing tensile stresses in FRP confinement which results in an increasing circumferential confinement pressure applied by FRP confinement to the confined concrete until the FRP confinement is ruptured. The circumferential confinement pressure applied by FRP confinement on the concrete at ultimate axial compressive load ($f_{l,a}$) is a function of material properties of FRP composite i.e., modulus of elasticity (E_{FRP}), thickness (t_{FRP}), circumferential rupture strain (ε_{rup}), and diameter of confined concrete (D) (Hadi *et al*. 2013, Ozbakkaloglu 2013) as given in Eq. (1)

$$f_{l,a} = \frac{2E_{FRP}t_{FRP}\varepsilon_{rup}}{D} \tag{1}$$

In this study, analytical axial load-axial deformation ($P - \delta$) curves were drawn to simulate experimental $P - \delta$ curves of CFFT columns with and without FRP bars. Columns CT and GT comprised FRP tube confined concrete. Columns CTCR and GTGR comprised FRP tube confined concrete reinforced with FRP bars.

The analytical $P - \delta$ curves of FRP tube confined concrete were drawn using the stress-strain ($f_c - \varepsilon$) model proposed by Samaan *et al*. (1998) for FRP confined concrete. The $f_c - \varepsilon$ model proposed by Samaan *et al*. (1998) is well suited to simulate experimental $P - \delta$ curves of CFFT columns with and without FRP bars as Samaan *et al*. (1998) model accounts for the effect of FRP confinement on both first and second ascending $f_c - \varepsilon$ curves. The $f_c - \varepsilon$ model of Samaan *et al*. (1998) for FRP confined concrete (Eq. (2)) is a modified version of versatile elastic-plastic $f_c - \varepsilon$ model developed by Richard and Abbott (1975) (Eq. (3)). Samaan *et al*. (1998) modified four parameters of Richard and Abbott (1975) $f_c - \varepsilon$ model using experimental results of FRP tube confined concrete cylinders, as given in Eq. (2)

$$f_c = \frac{(E_1 - E_2)\varepsilon_c}{(1 + (\frac{(E_1 - E_2)\varepsilon_c}{f_o})^n)^{1/n}} + E_2\varepsilon_c \tag{2}$$

where

$$E_1 = 3950\sqrt{f_{co}} \tag{3}$$

$$E_2 = 245.61 f_{co}^{\ 0.2} + 1.3456\frac{E_{FRP}t_{FRP}}{D} \tag{4}$$

$$f_o = 0.872 f_{co} + 0.371 f_{l,a} + 6.258 \tag{5}$$

$$f'_{cc} = f_{co} + 6 f_{l,a}^{\ 0.7} \tag{6}$$

$$\varepsilon_{cu} = \frac{f'_{cc} - f_o}{E_2} \tag{7}$$

where, f_c is the axial stress of FRP confined concrete, ε_c is the axial strain of FRP confined concrete, E_1 and E_2 are the first and second slopes of ascending $f_c - \varepsilon$ of FRP confined concrete, respectively, f_o is the axial stress at the intercept of second slope with the axial stress axis, n is a curve-shape parameter which controls the slope of the two rising $f_c - \varepsilon$ curves meeting in transition region, f'_{cc} is the FRP confined concrete strength and ε_{cu} is the ultimate FRP confined concrete strain. The f'_{cc} and ε_{cu} were used to analytically determine the peak axial load and peak axial deformation, respectively of the tested CFFT columns and also to construct analytical axial load-axial deformation curves.

Axial stress-strain ($f_c - \varepsilon$) behavior of FRP bar is linear elastic till rupture (Kobayashi and Fujisaki 1995; Deitz *et al*. 2003). In FRP bar, the axial stress (f_{FRP}) at any axial strain (ε_{FRP}) was calculated according to Eq. (8)

$$f_{FRP} = E_{FRP}\varepsilon_{FRP} \tag{8}$$

The analytical axial loads (P) and axial deformations (δ) of CFFT columns with and without FRP reinforcement at any axial stress (f_c) and axial strain (ε_c) were determined using Eqs. (9) and (10), respectively with appropriate strength reduction factors

$$P = f_c A_g + f_{fu,c} A_{FRP} \tag{9}$$

$$\delta = \varepsilon_c H \tag{10}$$

where A_g is the gross sectional area of CFFT column, $f_{fu,c}$ is the ultimate compressive strength of FRP bar, A_{FRP} is the cross-sectional area of FRP bars and H is the height of test column. A spread sheet was developed in MS-Excel to carry out the required computations and to draw the curves.

5. Comparison of experimental and analytical axial load-deformation curves

The analytical first and second rising axial load-axial deformation ($P - \delta$) curves of Columns CT and GT matched very well with the corresponding experimental first and second rising $P - \delta$ curves (Figs. 6(a) and (b)). For Columns CT and GT, axial compressive loads at the transition points of analytical $P - \delta$ curves were about 6.7% and 9.4% smaller, respectively, than the axial compressive loads at the transition points of the corresponding experimental $P - \delta$ curves. For Column CT, axial compressive load at the rupture point of the analytical $P - \delta$ curve was 2.3% smaller than the corresponding experimental $P - \delta$ curve. For Column GT, axial compressive load at the rupture point of the analytical $P - \delta$ curve was 4.7% larger than the corresponding experimental $P - \delta$ curve.

The axial compressive loads of analytical $P - \delta$ curve of Column CTCR were 3.3% and 7.6% larger at transition and rupture points, respectively, than the axial compressive

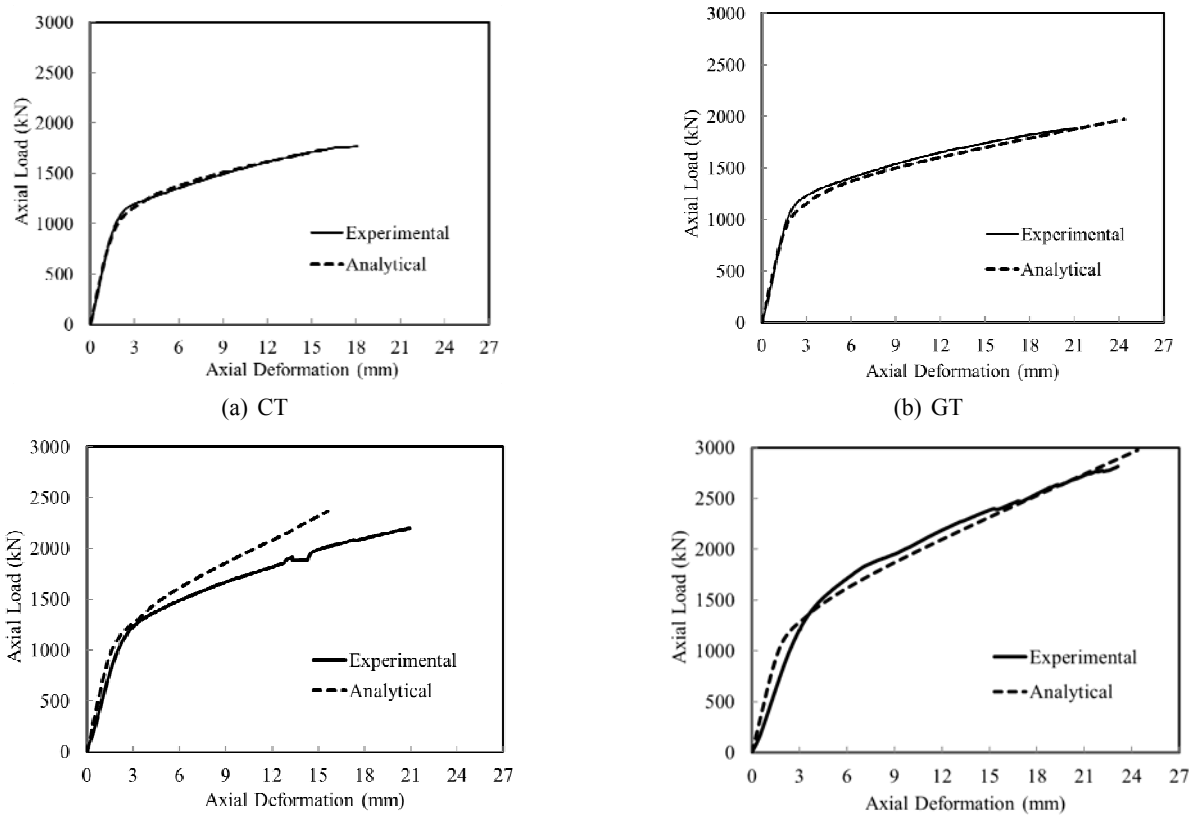

Fig. 6 Experimental and analytical axial load-axial deformation behaviour of Columns

loads of experimental $P - \delta$ curve. This is because CFRP bars might have slipped during the test due to inadequate bonding with surrounding concrete which resulted in the smaller experimental axial compressive load-deformation than the analytical axial compressive load-deformation (Fig. 6(c)). The axial compressive loads of analytical $P - \delta$ curve of Column GTGR were 8.1% and 5.8% larger at transition and rupture points, respectively, than the axial compressive loads of experimental $P - \delta$ curve. The difference between the experimental and analytical $P - \delta$ curves was attributed to stress concentration in Column GTGR which caused rupture at the top end of GFRP bars (Fig. 6(d)).

6. Theoretical axial load carrying capacity of CFFT

The ACI 318M-11 (2011) and CSA S806-12 (2012) define the nominal axial compressive load capacity (P_n) of steel RC column under axial load as

$$P_n = k_c f_{co}(A_g - A_s) + f_y A_s \quad (11)$$

where f_{co} is the 28-day compressive concrete cylinder strength, A_s and f_y are the area and yield strength of steel bars, respectively. In Eq. (11), the concrete strength and yield strength of steel bars are added to determine the theoretical P_n of short RC columns in pure axial compression. The column capacity can be determined based on Eq. (11), as both steel and concrete reach the plastic states at approximately the same strain level (Ozbakkaloglu and Saatcioglu 2004). The parameter k_c is a ratio of in-place concrete strength to concrete cylinder strength. The k_c incorporates the shape and size effect, and differences in concrete casting between columns and cylinders. In Eq. (11), the confinement effect of steel helical reinforcement is ignored. This was due to the observation that at the peak axial load the lateral strain in steel helix was about 15% of the yield strain of steel bar (Mohamed *et al*. 2014)

The ACI 318M-11 (2011) recommends k_c as 0.85 on the basis of test results of extensive experimental program performed on RC columns. In CSA S806-12 (2012) k_c is expressed as a function of f_{co} (Eq. (12)).

$$k_c = 0.85 - 0.0015 f_{co} \geq 0.67 \quad (12)$$

The k_c in Eq. (12) decreases from 0.85 to 0.67 with increase in f_{co} up to 120 MPa and remains constant for f_{co} greater than 120 MPa. The P_n of Column REF was calculated with Eq. (11) using k_c = 0.85 and 0.79 for f_{co} = 37 MPa in accordance with the recommendations in ACI 318M-11 (2011) and CSA S806-12 (2012), respectively. The axial compressive load capacity expressions in ACI 318M-11 (2011) and CSA S806-12 (2012) underestimated the P_n of Column REF by 10.1% and 14.3%, respectively.

The ACI 440.1R-06 (2006) does not suggest using FRP bars as longitudinal reinforcement in columns. In the latest edition of ACI 440.1R-15 (2015), the section suggesting against using of FRP bars as reinforcement in columns has

been excluded. Afifi *et al*. (2014a, b) reported the P_n of FRP bar RC column (Eq. (13)) similar to the guidelines of ACI 440.1R-06 (2006) by excluding the contribution of FRP bars in axial load carrying capacity and using $k_c = 0.85$ as

$$P_n = 0.85 f_{co}(A_g - A_{FRP}) \tag{13}$$

Although CSA S806-12 (2012) permits providing FRP bars as longitudinal reinforcement in columns under axial compression; however, it ignores the load carried by FRP bars in P_n. The CSA S806-12 (2012) uses a similar equation of the steel RC column to calculate the P_n of the FRP bar RC column by ignoring the contribution of FRP bar and using $k_c = 0.85 - 0.0015 f_{co} \geq 0.67$ as

$$P_n = k_c f_{co}(A_g - A_{FRP}) \tag{14}$$

Afifi *et al*. (2014a, b) conducted a series of experimental investigations to investigate the effect of longitudinal and helical reinforcements on P_n of FRP bar RC columns. Afifi *et al*. (2014a, b) reported that Eqs. (13) and (14) underestimated the axial compressive load capacity of FRP bar RC columns on average by 25-30% and 35-40%, respectively, by not considering the contribution of FRP bars as longitudinal reinforcement. Afifi *et al*. (2014a, b) reported that FRP bars in FRP bar RC columns effectively resisted the axial compression even after crushing of concrete and introduced Eq. (15) to calculate the axial compressive load capacity of FRP bar RC columns by taking into account the contribution of FRP bars.

$$P_n = 0.85 f_{co}(A_g - A_{FRP}) + \alpha_{FRP} f_{fu} A_{FRP} \tag{15}$$

where, A_{FRP} is the area of longitudinal FRP bar, f_{fu} is the ultimate tensile strength of FRP bar and α_{FRP} accounts for the lower compressive strength than tensile strength of FRP bar. Eq. (15) ignores the confinement effect of FRP helices in the P_n of FRP bar RC columns as the reported average lateral strain in the FRP helix at the peak axial load was about 2% of the ultimate tensile strain of FRP bar (Mohamed *et al*. 2014).

The ACI 440.2R-08 (2008) and CSA S806-12 (2012) use the same equation of the steel RC column (Eq. 11) to calculate the P_n of the externally FRP bonded steel RC column using f'_{cc} instead of f_{co} as confining RC column with FRP enhances the P_n of RC columns. The ACI 440.2R-08 (ACI 2008) adopts the stress-strain model proposed by Lam and Teng (2003) with minor modifications to calculate FRP confined concrete strength (f'_{cc}) given in Eq. (16).

$$f'_{cc} = f_{co} + \psi_f k_a 3.3 f_{l,a} \tag{16}$$

where ψ_f is a reduction factor and k_a is efficiency factor to account for the geometry of the section. The ACI 440.2R-08 (2008) recommends ψ_f as 0.95 and k_a as 1.0 for circular columns. The ACI 440.2R-08 (ACI 2008) limits the minimum value of circumferential confinement pressure at ultimate ($f_{l,a}$) to $0.08 f_{co}$ (i.e., $f_{l,a} \geq 0.073 f_{co}$) to ensure a rising second branch in the stress-strain performance (strain hardening behavior). Also, the maximum confined concrete strain (ε_{cu}) is limited to 0.01 to reduce cracking in confined concrete which may result in loss in the integrity of concrete.

The CSA S806-12 (2012) proposes Eq. (17) to calculate FRP confined concrete strength (f'_{cc}) as

$$f'_{cc} = 0.85 f_{co} + k_1 k_s f_{l,a} \tag{17}$$

where

$$k_1 = 6.7(f_{l,a}^{-0.17}) \tag{18}$$

where k_s incorporates the shape of the section and is equal to 1.0 for circular section. The CSA S806-12 (2012) limits the maximum value of FRP circumferential strain (ε_{rup}) to 0.004. It was observed that by limiting the FRP circumferential strain to 0.004, the calculated circumferential confinement pressures at ultimate axial load ($f_{l,a}$) (Eq. (1)) of CFRP-CFFT (Columns CT and CTCR) and GFRP-CFFT (Columns GT and GTGR) were only about 29% and 15%, respectively, of the experimental circumferential confinement pressures at ultimate axial load ($f_{l,a}$). Eq. (17) significantly underestimated the FRP confined concrete strength (f'_{cc}) of the tested columns. Hence, the CSA S806-12 (2012) underestimated the P_n of the tested columns.

This study proposes Eq. (19) to predict the axial compressive load capacity of CFFT columns with and without FRP bars based on the recommendations of ACI 440.2R-08 (2008) and Afifi *et al*. (2014a, b). The Eq. (19) adequately considers the confinement effect provided by FRP tube at peak axial load and contribution of FRP bars.

$$P_n = 0.85 f'_{cc}(A_g - A_{FRP}) + \alpha_{FRP} f_{fu} A_{FRP} \tag{19}$$

A reduction factor (α_{FRP}) of 0.52 for CFRP bars and 0.61 for GFRP bars was determined based on the mechanical properties of tested FRP bars in compression (Table 1) and tension (Table 2). In Eq. (19), f'_{cc} of the tested columns was calculated using Samaan *et al*. (1998) model (Eq. (6)). Eq. (19) underestimated the experimental axial load carrying capacity of Columns CT, GT and GTGR by about 12.4% as given in Table 5.

However, Column CTCR exhibited higher calculated axial compressive load capacity than experimental axial compressive load capacity as CFRP bars did not develop an adequate bond with surrounding concrete. Moreover, the axial compressive load capacity of Columns CT, GT, CTCR and GTGR was calculated by not accounting for the confinement effect provided by CFRP and GFRP tubes (using f_{co} instead of f'_{cc}), using Eq. (15) which significantly underestimated the experimental axial compressive load capacity of the tested columns by about 40.9%. It was observed that the measured average circumferential strains in tested CFRP tubes and GFRP tubes at peak axial compressive loads were about 61% and 27%, respectively, of the ultimate tensile strain in FRP tubes which were significantly higher than the measured lateral strain in FRP helices reported in Afifi *et al*. (2014a). Based on the

Table 5 Comparison of experimental and analytical axial load capacities of tested CFFT columns

Col. ID	Exp. (P), kN	Cal. P with Eq. (19)	Difference between Exp. and Cal. (Eq. (19)) (%)	Cal. P with Eqn. (15)	Difference between Exp. and Cal. (Eq. (15)) (%)
CT	1770	1425.9	-19.4	1062.9	-25.5
GT	1884	1673.4	-11.2	1136.5	-39.7
CTCR	2197	2273.4	+3.5	1307.2	-40.5
GTGR	2812	2629.2	-6.5	1184.4	-57.9

experimental results of columns tested in this study, it is suggested that the confinement effect of FRP tube needs to be considered in calculating the axial compressive load capacity of CFFT columns with and without FRP bars.

7. Conclusions

This study presented experimental and analytical investigation results of unreinforced CFFT columns (CT and GT) and CFFT columns reinforced with FRP bars (CTCR and GTGR) under concentric axial compression. A reference steel RC (REF) column was also tested under concentric axial compression. The following conclusions are drawn on the basis of experimental and analytical investigations conducted in this research study:

- Column CTCR carried 24.3% larger axial compressive load capacity than Column CT and Column GTGR carried 49.3% larger axial compressive load capacity than Column GT. The CFRP bars contributed to 11.7% of the axial compressive load capacity of Column CTCR and GFRP bars contributed to 12.5% of the axial compressive load capacity of Column GTGR. Moreover, Column CTCR exhibited 15.4% larger axial deformations than Column CT and Column GTGR exhibited 8.5% larger axial deformations at peak axial compressive load than Column GT at peak axial loads.
- The analytical axial load-axial deformation curves of CFFT columns with and without FRP bars matched well with the experimental axial load-axial deformation curves.
- An equation is proposed based on the experimental investigations reported in this study to calculate the axial compressive load capacity of unreinforced and FRP bar reinforced CFFT columns by taking into account the confining effect of FRP tube and reduced effectiveness of FRP bar at peak axial load. The results of the proposed equation matched well with the experimental results.
- Founded on experimental and analytical results of the columns reported in this study, CFFT can serve as a substitute of the conventional steel RC column under concentric axial compression in coastal areas where rusting of steel is a key concern.

Acknowledgments

The authors acknowledge the UOW, Australia for providing the facilities and funding to successfully conduct the experiments presented in this research. The first author acknowledges the University of Engineering and Technology, Lahore and Higher Education Commission (HEC) of Pakistan, and the UOW, Australia for funding his PhD studies.

References

ACI 318M-11 (2011), Building code requirements for structural concrete and commentary; American Concrete Institute. Farmington Hills, MI 48331, USA.

ACI 440.1R-06 (2006), Guide for the design and construction of structural concrete reinforced with FRP bars; American Concrete Institute, USA.

ACI 440.2R-08 (2008), Guide for the design and construction of externally bonded FRP systems for strengthening concrete structures; American Concrete Institute, USA.

ACI 440.1R-15 (2015), Guide for the design and construction of structural concrete reinforced with FRP bars; American Concrete Institute, USA.

Afifi, M., Mohamed, H. and Benmokrane, B. (2014a), "Axial capacity of circular concrete columns reinforced with GFRP bars and spirals", *J. Compos. Constr.*, **18**(1), 04013017.

Afifi, M., Mohamed, H. and Benmokrane, B. (2014b), "Strength and axial behaviour of circular concrete columns reinforced with CFRP bars and spirals", *J. Compos. Constr.*, **18**(2), 04013035.

Alsayed, S.H., Al-Salloum, Y.A., Almusallam, T.H. and Amjad, M.A. (1999), "Concrete columns reinforced by GFRP Rods", *Proceedings of the FRPRCS-4*.

AS 1012.9-1999 (1999), Methods of testing concrete, Method 9: Determination of the compressive strength of concrete specimens; Standards Australia. Sydney, Australia.

AS 1391-2007 (2007), Metallic materials - Tensile testing at ambient temperature, Standards Australia, Sydney, Australia.

ASTM D695-10 (2010), Standard Test Method for Compressive Properties of Rigid Plastics; American Society for Testing and Materials, 100 Barr Harbor Drive, PO Box C700, West Conshohocken, PA 19428-2959, USA.

ASTM D7205/D7205M-11 (2011), Standard Test Method for tensile properties of Fibre Reinforced Polymer Matrix Composite Bars; American Society for Testing and Materials, 100 Barr Harbor Drive, PO Box C700, West Conshohocken, PA 19428-2959: USA.

Aslani, F., Uy, B., Tao, Z. and Mashiri, F. (2015), "Predicting the axial load capacity of high strength concrete filled steel tubular columns", *Steel Compos. Struct., Int. J.*, **19**(4), 967-999.

Chaallal, O. and Benmokrane, B. (1993), "Physical and mechanical performance of an innovative glass fibre reinforced

plastic rod", *Can. J. Civil Eng.*, **20**(2), 254-268.
CSA-S806-12 (2012), Design and construction of building components with fibre reinforced polymers; Canadian Standards Association, ON, Canada.
CST (2014), CST COMPOSITES, Caringbah NSW 1495, Australia. URL: http://www.cstcomposites.com/products-and-services/tubes-rods-and-components/
Deitz, D., Harik, I. and Gesund, H. (2003), "Physical properties of glass fibre reinforced polymer rebars in compression", *J. Compos. Constr.*, **7**(4), 363-366.
De Luca, A., Matta, F. and Nanni, A. (2010), "Behaviour of full scale glass fibre reinforced polymer reinforced concrete columns under axial load", *ACI Struct. J.*, **107**(5), 589-596.
Hadhood, A., Mohamed, H. and Benmokrane, B. (2016), "Axial load-moment interaction diagram of circular concrete columns reinforced with CFRP bars and spirals: Experimental and theoretical investigations", *J. Compos. Constr.*
Hadi, M.N.S., Pham, T. and Lei, X. (2013), "New method of strengthening reinforced concrete square columns by circularizing and wrapping with Fibre-Reinforced Polymer or Steel Straps", *J. Compos. Constr.*, **17**(2), 229-238.
Hadi, M.N.S., Khan, Q.S. and Sheikh, M.N. (2016), "Axial and flexural behaviour of unreinforced and FRP bar reinforced circular concrete filled FRP tube columns", *Constr. Build. Mater.*, **122**, 43-53.
Hadi, M.N.S., Karim, H. and Sheikh, M.N. (2017), "Experimental investigations on circular concrete columns reinforced with GFRP bars and helices under different loading conditions", *J. Compos. Constr.*
Hong, W.K. and Kim, C. (2004), "Behaviour of concrete columns confined by carbon composites tubes", *Can. J. Civil Eng.*, **31**(2), 178-188.
ISO 10406-1-15 (2015), Fibre reinforced polymer (FRP) reinforcement of concrete - Test methods - Part 1: FRP bars and grids; International Standard, Switzerland.
Khan, Q.S., Sheikh, M.N. and Hadi, M.N.S. (2016), "Axial compressive behaviour of circular CFFT: Experimental database and design-oriented model", *Steel Compos. Struct., Int. J.*, **21**(4), 921-947.
Khan, Q.S., Sheikh, M.N. and Hadi, M. (2017), "Axial-Flexural interactions of GFRP-CFFT columns with and without reinforcing GFRP bars", *J. Compos. Constr.*, **21**(3), 04016109.
Khan, Q.S., Sheikh, M.N. and Hadi, M. (2018a), "Predicting strength and strain enhancement ratios of circular fiber-reinforced polymer tube confined concrete under axial compression using artificial neural networks", *Adv. Struct. Eng.*, 1-18.
Khan, Q.S., Sheikh, M.N. and Hadi, M. (2018b), "Concrete filled carbon FRP tube (CFRP-CFFT) columns with and without CFRP reinforcing bars: Axial and flexural interactions", *J. Compos. Part B: Eng.*, **133**, 42-52.
Kobayashi, K. and Fujisaki, T. (1995), "Compressive behaviour of FRP reinforcement in non-prestressed concrete members", *Proceedings of the Second International RILEM Symposium* (*FRPRCS-2*), L.Taerwe, Editor.
Lam, L. and Teng, J.G. (2003), "Design-oriented stress–strain model for FRP-confined concrete", *Constr. Build. Mater.*, **17**(6-7), 471-489.
Mirmiran, A., Shahawy, M., Samaan, M., El Echary, H., Mastrapa, J.C. and Pico, O. (1998), "Effect of column parameters on FRP confined concrete", *J. Compos. Constr.*, **2**(4), 175-185.
Mohamed, H. and Masmoudi, R. (2008), "Compressive behaviour of reinforced concrete filled FRP tubes", ACI-SP, SP-257, 91-108.
Mohamed, H. and Masmoudi, R. (2010), "Axial load capacity of concrete-filled FRP tube columns: Experimental versus theoretical predictions", *J. Compos. Constr.*, **14**(2), 231-243.
Mohamed, H.M., Afifi, M.Z. and Benmokrane, B. (2014), "Performance evaluation of concrete columns reinforced longitudinally with FRP bars and confined with FRP hoops and spirals under axial load", *J. Bridge Eng.*, **19**(7), 04014020.
Ozbakkaloglu, T. (2013), "Compressive behaviour of concrete-filled FRP tube columns: Assessment of critical column parameters", *Eng. Struct.*, **51**, 188-199.
Ozbakkaloglu, T. and Oehlers, D.J. (2008), "Concrete filled square and rectangular FRP Tubes under axial compression", *J. Compos. Constr.*, **12**(4), 469-477.
Ozbakkaloglu, T. and Saatcioglu, M. (2004), "Rectangular stress block for high strength concrete", *ACI Struct. J.*, **101**(4), 475-483.
Ozbakkaloglu, T. and Vincent, T. (2013), "Axial compressive behaviour of circular high strength concrete filled FRP tubes", *J. Compos. Constr.*, 04013037-1-11.
Pantelides, C., Gibbons, M. and Reaveley, L. (2013), "Axial load behaviour of concrete columns confined with GFRP spirals", *J. Compos. Constr.*, **17**(3), 305-313.
Park, J. and Yoo, J. (2015), "Flexural and compression behavior for steel structures strengthened with Carbon Fiber Reinforced Polymers (CFRPs) sheet", *Steel Compos. Struct., Int. J.*, **19**(2), 441-465.
Park, J.H., Jo, B.W., Yoon, S.J. and Park, S.K. (2011), "Experimental investigation on the structural behaviour of concrete filled FRP tubes with/without steel rebar", *KSCE J. Civil Eng.*, **15**, 337-345.
Ramezanpour, M., Morshed, R. and Eslami, A. (2018), "Experimental investigation on optimal shear strengthening of RC beams using NSM GFRP bars", *Struct. Eng. Mech., Int. J.*, **67**(1), 45-52.
Richard, R.M. and Abbott, B.J. (1975), "Versatile elastic plastic stress strain formula", *J. Eng. Mech. Div.*, **101**, 511-515.
Samaan, M., Mirmiran, A. and Shahawy, M. (1998), Model of concrete confined by Fibre composites", *J. Struct. Eng.*, **124**(9), 1025-1031.
Shahraki, M., Sohrabi, M.R., Azizyan, G.R. and Narmashiri, K. (2018), "Experimental and numerical investigation of strengthened deficient steel SHS columns under axial compressive loads", *Struct. Eng. Mech., Int. J.*, **67**(2), 207-217.
Thomas, J. and Ramadass, S. (2015), "Design for shear strength of concrete beams longitudinally reinforced with GFRP bars", *Struct. Eng. Mech., Int. J.*, **53**(1), 41-55.
Tobbi, H., Farghaly, A.S. and Benmokrane, B. (2012), "Concrete columns reinforced longitudinally and transversally with glass Fibre-Reinforced Polymer bars", *ACI Struct. J.*, **109**(4), 551-558.
Vincent, T. and Ozbakkaloglu, T. (2013a), "Influence of concrete strength and confinement method on axial compressive behaviour of FRP confined high and ultra-high strength concrete", *Compos. Part B: Eng.*, **50**, 413-428.
Vincent, T. and Ozbakkaloglu, T. (2013b), "Influence of fibre orientation and specimen end condition on axial compressive behaviour of FRP confined concrete", *Constr. Build. Mater.*, **47**, 814-826.
V-ROD (2012), Composite reinforcing rods technical data sheet, Largs Bay, SA, Australia.
Wang, W., Sheikh, M.N., Hadi, M.N.S., Gao, D. and Chen, G. (2017), "Behaviour of concrete encased concrete filled FRP tube (CCFT) columns under axial compression", *Eng. Struct.*, **147**, 256-268.
Wang, W., Martin, P.R., Sheikh, M.N. and Hadi, M.N.S. (2018), "Eccentrically loaded FRP confined concrete with different wrapping schemes", *J. Compos. Constr.*, **22**(6), 04018056.

BU